

Stability of the double gyroid phase to nanoparticle polydispersity in polymer-tethered nanosphere systems†

Carolyn L. Phillips,^a Christopher R. Iacovella^b and Sharon C. Glotzer^{*abc}

Received 8th June 2009, Accepted 8th January 2010

First published as an Advance Article on the web 24th February 2010

DOI: 10.1039/b911140a

Recent simulations predict that aggregating nanospheres functionalized with polymer “tethers” can self-assemble to form the double gyroid (DG) phase seen in block copolymer and surfactant systems. Within the struts of the gyroid, the nanoparticles pack in icosahedral motifs, stabilizing the gyroid phase in a small region of the phase diagram. Here, we study the impact of nanoparticle size polydispersity on the stability of the double gyroid phase. We show for low amounts of polydispersity the energy of the double gyroid phase is lowered. A large amount of polydispersity raises the energy of the system, disrupts the icosahedral packing, and eventually destabilizes the gyroid. Our results show that the DG forms readily up to 10% polydispersity. Considering polydispersity as high as 30%, our results suggest no terminal polydispersity for the DG, but that higher polydispersities may kinetically inhibit the formation of phase. The inclusion of a small population of either smaller or larger nanospheres encourages low-energy icosahedral clusters and increases the gyroid stability while facilitating its formation. We also introduce a new measure for determining the volume of a component in a microphase-separated system based on the Voronoi tessellation.

I. Introduction

The ability of block copolymers to self assemble into systems with periodic micro-domains makes them attractive building blocks for engineering self-assembled nanomaterials.^{1–3} Possible applications of the periodic nanometre-sized domains include microelectronics⁴ and high-density storage media,⁵ photonic band gap materials,^{6,7} and drug delivery systems.^{8,9} Recent attention has focused on the use of polymer-tethered nanoparticles as a means to create novel nano-materials by exploiting the block copolymer-like immiscibility between the nanoparticle and tether.^{10–14} Several techniques exist to create composite polymer-nanoparticles. Westenhoff and Kotov, for example, used poly(ethyleneglycole) PEG polymer to tether a CdTe nanoparticle to a surface.¹⁵ Several research groups have created gold or SiO₂ nanoparticles functionalized with polymers or DNA linkers.^{16–18} Even more advanced techniques are being proposed to create nanoparticles with multiple functionalizations with controlled placements for creating self-assembled structures.^{19,20} Polymer tethered nanosphere amphiphiles are, therefore, currently realizable. Iacovella and coworkers^{21–23} predicted using computer simulations that polymer-tethered nanospheres (NS) (Fig. 1a), under suitable conditions, form phases similar to block copolymers,^{24–26} including the double gyroid (DG) phase. The DG (Fig. 1b) is a triply periodic structure of space group Ia3d where space is divided into three regions: two interpenetrating

but identical networks (here, the NS domain) and a matrix (polymer tether domain). The surface separating the domains is approximately a surface of constant mean curvature and minimizes the interfacial area subject to a volume constraint.²⁷

The DG predicted by Iacovella, *et al.* was formed in simulations of monodisperse tethered nanospheres (TNS), that is, TNS with a uniform diameter NS. In most nanoparticle synthesis approaches, the level of polydispersity is non-zero, and in some cases can be appreciable. State-of-the-art techniques are able to achieve nanoparticles with polydispersity values as low as 6%.^{28–30} For other self-assembling liquid crystal or hard sphere systems, it has been recognized that certain crystalline structures can only tolerate a certain level of polydispersity and still be a stable phase; that is, they exhibit terminal polydispersity.³¹ For example, Pusey (1987) argued that crystallization of hard sphere colloids would have a terminal polydispersity between 6–11%,³² a range supported by subsequent experiments.³³ Terminal polydispersity for different systems has been studied experimentally,³⁴

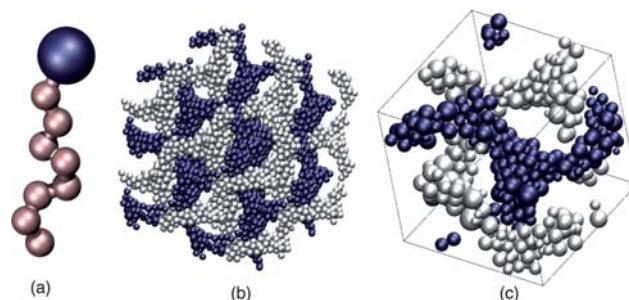


Fig. 1 (a) A single tethered nanosphere (TNS), (b) Eight unit cells of a monodisperse gyroid and (c) a single unit cell of a 24% polydisperse gyroid. Tethers are omitted in (b) and (c). The two interweaving gyroid domains are colored blue and grey to show the separate bicontinuous structure, but are composed of identical NS.

^aApplied Physics Program, University of Michigan, Ann Arbor, Michigan, 48109, USA

^bDepartment of Chemical Engineering, University of Michigan, Ann Arbor, Michigan, 48109, USA

^cDepartment of Materials Science and Engineering, University of Michigan, Ann Arbor, Michigan, 48109, USA

† Electronic supplementary information (ESI) available: Fig. S1–S4. See DOI: 10.1039/b911140a

analytically,³⁵ and computationally.^{31,36} The sensitivity of the DG phase to polydispersity in nanosphere diameter may very well determine the cost and method of manufacturing TNS capable of forming this phase, or even the likelihood of ever obtaining the DG phase under non-idealized conditions. Iacovella *et al.*^{22,23} suggested that the stability of the DG phase for tethered nanoparticles is linked to the ability of the nanoparticles to locally order into low energy motifs. Specifically, it was found that the nanospheres locally formed icosahedral structures with partial coordination. While icosahedral local packing may be an ideal stable configuration for same size spheres, the addition of polydispersity will undoubtedly frustrate icosahedral packing, potentially affecting the overall stability of the structure.

In this paper, we seek to determine the role polydispersity plays in the formation of the DG structure for a system of TNS. We will investigate how much polydispersity the DG phase can tolerate before it ceases to be a free energy minimum for the TNS system. We also seek to understand by what mechanism increasing polydispersity destabilizes the gyroid phase as this may point to compensating strategies. In section II of this paper, we describe the method we use to model polydisperse TNS. In section III we describe the analytical techniques we use to study the packing properties of polydisperse nanospheres, namely (1) the structure factor calculation designed to identify the unique peaks associated with the DG structure in a single unit cell, (2) the R_{YLM} structure analysis used to identify the local ordering of particles within the DG, and (3) the Voronoi tessellation, extended to handle polydisperse spheres and used to identify how increasing the polydispersity affects the net packing of nanospheres in the DG structure. This third technique represents, to our knowledge, the first use of a Voronoi tessellation in this context and a more detailed consideration of this technique is provided in the supplemental materials. In section IV we present the results of our simulations and analysis. In subsection IV.A, we explore polydispersity both by “growing” polydispersity into “pre-assembled” DG structures formed from ideal TNS, and by cooling polydisperse TNS from a disordered initial condition. Using these two methods we consider the impact of polydispersity on the DG. In section IV.B, we discuss the impact of polydispersity on the free energy of the system. In subsection IV.C, we use the R_{YLM} structure analysis to determine how polydispersity affects the local icosahedral packing in the DG and analyze why a low level of polydispersity promotes local icosahedral structure in the DG. In subsection IV.D, we use an extended Voronoi tessellation, the radical tessellation, to measure the impact of polydispersity on the packing fraction in the DG domain and on the average NS coordination number. In section V we provide concluding remarks.

II. Simulation model and method

A. Model

We utilize a minimal coarse-grained molecular model to study the phase behavior of tethered NS, the same model used by Iacovella *et al.*²² NS are modeled as beads with average diameter 2.0σ connected to tethers *via* a finitely extensible non-linear elastic (FENE) spring.³⁷ Tethers are modeled as bead-spring chains containing eight beads of diameter σ connected *via* FENE springs. Interactions between beads

and NS are modeled using empirical pair potentials. The model captures the geometry of the nanoparticles, immiscibility between tether and nanoparticles, and flexibility of the polymer tether.

Solvent selectivity is modeled by assuming that at sufficiently low T the solvent is poor for the NS but good for the tethers, resulting in a condition where nanoparticles will tend to aggregate. The effective attraction between two nanoparticles of diameters σ_i and σ_j is modeled using a radially shifted 12-6 Lennard-Jones potential (LJ), which is also truncated and shifted to zero at r_{cutoff} ,

$$U_{LJS} = \begin{cases} 4\epsilon \left(\left(\frac{\sigma}{r - \alpha_{ij}} \right)^{12} - \left(\frac{\sigma}{r - \alpha_{ij}} \right)^6 \right) - 4\epsilon \left(\left(\frac{\sigma}{2.5} \right)^{12} - \left(\frac{\sigma}{2.5} \right)^6 \right) & r < r_{\text{cutoff}} \\ 0 & r \geq r_{\text{cutoff}} \end{cases} \quad (1)$$

where $r_{\text{cutoff}} = 2.5\sigma + \alpha_{ij}$, and $\alpha_{ij} = (\sigma_i + \sigma_j)/2 - \sigma$. The effect of the radially shifted Lennard-Jones potential is to fix the range of the potential and location of the attractive well with respect to the NS surface; the potential well minimum is the same distance from the surface of the NS for all sizes of NS. If the attraction between particles is the result of solvent selectivity, then this functional form is a reasonable assumption, as attraction will be a short ranged interaction not strongly affected by small changes in the particle size.³⁸

All solvophilic tether beads interact *via* a purely repulsive Weeks-Chandler-Andersen (WCA) soft-sphere potential⁵⁴ to account for short-range, excluded volume interactions,

$$U_{WCA} = \begin{cases} 4\epsilon \left(\left(\frac{\sigma}{r - \alpha_{ij}} \right)^{12} - \left(\frac{\sigma}{r - \alpha_{ij}} \right)^6 \right) + \epsilon & r < r_{\text{cutoff}} \\ 0 & r \geq r_{\text{cutoff}} \end{cases} \quad (2)$$

where $\sigma_i = \sigma_j = \sigma$ (that is, $\alpha_{ij} = 0$) and $r_{\text{cutoff}} = 2^{1/6}\sigma$. NS-tether interactions are also treated with the purely repulsive WCA soft-sphere potential to account for short-range, excluded volume interactions, modeled using eqn (2) with $\sigma_{\text{tether}} = \sigma$ and $r_{\text{cutoff}} = 2^{1/6}\sigma + \alpha_{ij}$.

The natural units of this system are σ , the diameter of the tether bead; m_{tether} , the mass of a tether bead; and ϵ , the Lennard-Jones well depth. Bulk system volume fraction, ϕ , is defined as the ratio of volume of the beads to the system volume, the dimensionless time is $t^* = \sigma\sqrt{m/\epsilon}$, and the degree of immiscibility and solvent quality are determined by the dimensionless temperature, $T^* = k_B T/\epsilon$, where T is fixed at 1.0 and ϵ is varied to set T^* , unless otherwise indicated.

B. Method

We use Brownian dynamics (BD) to simulate the assembly of the TNS, which is described in detail in ref. 10,21,23. In BD, each bead is subjected to conservative, random and drag forces, and its motion is governed by the Langevin equation. For this system, the drag force scales with the size of the particle.

A set of polydisperse NS is created by sampling from a Gaussian distribution of particle diameters σ :

$$P(\sigma) = \frac{1}{\delta\sqrt{2\pi}} \exp \left[-\frac{1}{2} \left(\frac{\sigma - \bar{\sigma}}{\delta} \right)^2 \right] \quad (3)$$

The non-dimensionalized polydispersity, Δ , is defined as $100 \delta/\sigma$. Normally distributed populations of diameters are

generated. The population of diameters is then shifted so that the net volume of the nanoparticles is kept constant in order to prevent the bulk system volume fraction from deviating as polydispersity is introduced. The diameter distribution is also truncated at a minimum value of 1.0 so that all the NS are at least as large as a tether bead. The NS are polydisperse in size only. The mass of each nanoparticle is kept fixed at $m_{nanoparticle} = 27m_{tether}$ to minimize the number of variables in the system. Since any simulation contains a finite set of NS drawn from this distribution (typically 505 for the volume fractions studied here), the nominal polydispersity of the distribution, *i.e.* the polydispersity of the distribution being sampled, and the actual polydispersity of the set generated differ slightly. In this paper, the nominal polydispersity of the distribution is presented as an integer value. When the polydispersity has a decimal component, this represents the actual polydispersity of the distribution. Polydispersity values reported on plots are actual Δ values.

C. Methods for introducing polydispersity

To study the impact of polydispersity on the stability of the DG phase, we use two methods that tend to stabilize the ordered or disordered state, respectively. A third method is used to study the impact of polydispersity as a continuous variable on the DG phase.

To generate the upper bound on a terminal polydispersity, if one exists, we artificially create “polydisperse DGs” starting from a “monodisperse DG”, that is, a DG composed of a monodisperse set of NS, by “growing” a polydisperse set of NS from a monodisperse set. Starting at $T^* = 0.256$, well below the order-disorder temperature, we slowly modify the radii of the nanoparticles until they match the target radii generated from a prescribed Gaussian distribution. We change the size of a particle during a simulation under the constraint that the change is done slowly relative to the time step of the simulation. The system is allowed to equilibrate for several million time steps, and then we observe whether the system remained within the DG structure. We then raise T^* slowly, allowing the potential energy to equilibrate for several million time steps at each T^* before heating again, until the polydisperse gyroids finally reach the order-disorder transition. This provides a rapid method to determine a rough estimate of the level of polydispersity that destabilizes the structure and what trends to expect for a self-assembled polydisperse gyroid structure. This method is considered to be the upper limit for finding polydisperse ordered structures as we are likely to form kinetically arrested structures; that is, the system may be trapped in a local free energy minimum and unable to evolve to a global free energy minimum. All DGs generated by this method will be referred to as artificially grown (AG) double gyroids.

To generate a lower bound for terminal polydispersity, we incrementally cool the polydisperse system from random initial conditions. We initialize a system with a polydisperse set of TNS at a high temperature, disordered state, and subsequently allow the system to run for several million time steps at decreasing temperatures. We cool the system until an ordered state is achieved. If a DG self-assembles repeatedly at a given polydispersity but not higher, then we consider that level of polydispersity to represent a lower bound for the terminal polydispersity, DGs

formed by this method will be referred to as self-assembled (SA) double gyroids.

To determine the stability of the DG phase across a range of polydispersities, Δ , and system volume fractions, ϕ , we initialize SA systems with ϕ in the range of 0.285 to 0.315, or 5% above and below where the DG phase was found for the monodisperse case in Iacovella 2007.²² At each ϕ , most of the simulations are run with identical box dimensions ($L = 23.8\sigma$). A few simulations are run varying the box dimension by $\pm 1\%$. Polydispersities of 0 to 30% are investigated with 10 independent simulations per state point. At each state point, the system is equilibrated at a high temperature and then follows a cooling schedule of 6×10^6 time steps at $T^* = 0.32$, 50×10^6 time steps at $T^* = 0.31$, 50×10^6 time steps at $T^* = 0.3$, 20×10^6 time steps at $T^* = 0.29$, 20×10^6 time steps at $T^* = 0.28$, 6×10^6 time steps at $T^* = 0.25$. For these simulations T rather than ε is adjusted to change the dimensionless temperature T^* for coding convenience. For $\Delta = 25\%$ and 30%, a separate cooling schedule is also used (50×10^6 time steps at $T^* = 0.27$, 50×10^6 time steps at $T^* = 0.26$, 50×10^6 time steps at $T^* = 0.25$, 50×10^6 time steps at $T^* = 0.24$).

To study Δ as a continuous variable, polydispersity is continuously added to the NS extremely slowly, or quasi-statically. The polydispersity is changed slowly enough that the system is able to relax in response to the change and the properties of the system, calculated as a function of time, closely approximate those of the equilibrated system. This is evident, as when polydispersity is subsequently removed from the system at the same rate, there is a minimal amount of hysteresis in the calculated properties. This is also verified by comparing the properties of equilibrated systems at fixed polydispersity values. Thus, the properties of this system, quasi-equilibrated over a continuous polydispersity range, approximate the average values of a collection of systems equilibrated at each polydispersity level. For this system, polydispersity is added at a rate of $2.385 \times 10^{-6} \Delta/\text{time-step}$ to a $\Delta = 23.85\%$ and then removed from the NS at the same rate until reaching a monodisperse state, all while holding the reduced temperature constant at $T^* = 0.256$.

As shown in Section IV, the properties of the DG produced by the three methods are consistent and in good agreement.

D. Computational resources

Simulations used locally authored code and the GPU-based HOOMD-Blue code package under development in our group, which permitted rapid exploration of the phase diagram. The latter simulations were run on our GPU cluster at the University of Michigan and on the 32-node GPU cluster, AC, at the National Center for Supercomputing Applications on NVIDIA Tesla S1070s. The former simulations using our CPU-based code were run on 2.0 Ghz G5 nodes at the University of Michigan and 2.2 Ghz Opteron Nodes (Jacquard Cluster at National Energy Research Scientific Computing Center). Roughly 800 independent simulations were investigated over 100,000 CPU (or GPU) hours.

III. Analysis methods

A. Identification of the double gyroid phase

To identify the DG structure in our simulations we calculate the structure factor in addition to using visual inspection. The

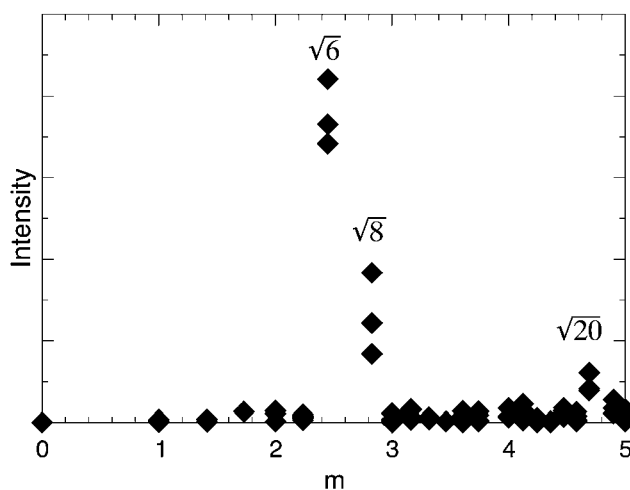


Fig. 2 The structure factor of a double gyroid with 20% polydispersity is shown as a function of m , the modulus of the integer wavelengths scaled wave vector, which is independent of the unit cell size. The characteristic gyroid peaks at $\sqrt{6}$, $\sqrt{8}$ and $\sqrt{20}$ are clearly visible.

structure factor in a simulation cell with a periodic structure is calculated following Schultz³⁹ for the nanoparticle component of the system:

$$S(\mathbf{q}) = \frac{\left(\sum_j \cos(\mathbf{q} \cdot \vec{r}_j)\right)^2 + \left(\sum_j \sin(\mathbf{q} \cdot \vec{r}_j)\right)^2}{N}$$

where the wave vector, \mathbf{q} , is restricted to an integer number of wavelengths within the simulation box, $\mathbf{q} = 2\pi \left(\frac{n_x}{L_x}, \frac{n_y}{L_y}, \frac{n_z}{L_z}\right)$. A structure is considered to be the DG if peaks are identified at $m = \sqrt{6}$ and $\sqrt{8}$ ^{24,25,40} where $m = \sqrt{n_x^2 + n_y^2 + n_z^2}$ (Fig. 2). Peaks at higher frequencies that are also associated with the DG, namely $\sqrt{20}$ and $\sqrt{22}$, were generally not clearly visible in our systems as they were obscured by noise in the structure factor, however excluding these higher order peaks is reasonable as our calculations are supplemented by visual inspection.

B. R_{YLM} local structure analysis: Spherical harmonics

To analyze the local configurations of the nanospheres, we utilize the R_{YLM} local structure analysis first introduced in Ref. 22 and further discussed in Ref. 23. The R_{YLM} method relies on creating a rotationally invariant spherical harmonic fingerprint of the central particle of a cluster of particles (for harmonics $L = 4, 6, \dots, 12$)⁴¹ and then matching this fingerprint to a library of known structures.^{22,23} A cluster is identified as the reference configuration that minimizes the residual value, R , where

$R = \sqrt{\sum_{i=4}^{12} (Q_i - Q_{ref})^2 + \sum_{i=4}^{12} (w_i - w_{ref})^2}$ or it is classified as disordered if it exceeds a certain cutoff. In the definition of R , Q_i and w_i are two metrics of local ordering based on evaluating a set of spherical harmonic functions $Y_{lm}(\theta, \phi)$ and defined in Steinhart *et al.*⁴¹ For our system, the local packing of nanospheres is divided into “clusters” by grouping each NS and its nearest-neighbor nanospheres, which define the coordination of the NS. Nearest neighbors are considered to be those with

a surface-to-surface distance less than or equal to 0.5σ , such that each neighbor would be within the potential well of the central NS. In turn, each NS in the system is considered as a central NS to determine the distribution of cluster types. This method characterizes the bond angles in the local structures rather than the radial distance, which is considered indirectly in $S(\mathbf{q})$. The R_{YLM} method permits recognition of the fact that the internal structure of a domain may be composed of many different local structures, not just one dominant structure type.

In general, local structures are characterized by which “family” they belong to, namely icosahedral (Z12), Frank-Kasper polyhedra (excluding icosahedra Z12), crystalline, or disordered. Each family of structure types contains multiple reference structures with different coordination numbers. To characterize local icosahedral packing, we incorporated into our reference database a series of partial icosahedral clusters that maintain the same bond angles as the full icosahedral cluster, but with 0–4 particles removed. These local structures are almost identical to the LJ minimum potential energy clusters found by Wales and Doye,⁴² which were also included in the reference database. The local structure is considered to be icosahedral if it matches the partial clusters from Wales and Doye⁴² or a partial icosahedral cluster.

We also include a family of Frank-Kasper (FK) polyhedra with coordinations 8 through 16, referred to as ZN, where N is the coordination number. The Z12 structure is the basis of the icosahedral family. Partial Frank-Kasper polyhedra were not included, as these local configurations, in practice, generally have similar structure and thus similar spherical harmonic fingerprints to partial icosahedra. The library also includes a family of crystalline structures composed of full and partial coordination clusters with face-centered-cubic (fcc) and hexagonal-close-packed bond angles (hcp).

The local structure of the DG was analyzed under two thermodynamic conditions, at $T^* = 0.256$ with a residual cutoff of 0.2, and quenched to $T^* = 0.02$ with a residual cutoff of 0.1. With these cutoffs, any cluster with $R > 0.2$ or 0.1, respectively, is considered disordered. These cutoffs were chosen to reduce the inclusion of disordered local structures. When the system is rapidly quenched to $T^* = 0.02$, the nanospheres become kinetically trapped in place, but still oscillate around their bond-angle position so the fraction of local structures found is time averaged over 250 dimensionless units of time while quenched. All values shown are averaged over 50–60 instances of the system separated by at least 500 units of time at $T^* = 0.256$, sufficient time for each particle in the system to have moved a distance of at least its radius.

C. Voronoi tessellation

To examine packing density (compactness) and nearest neighbor trends as a function of polydispersity we use an extension of the Voronoi tessellation. The Voronoi cell around a point is generally defined as the region of space that is closer to the given point than any other point. In a three-dimensional space, the Voronoi tessellation for a set of points uniquely divides the space into irregular polyhedra with flat faces and straight edges. If each point is the center of a sphere in a system of non-overlapping monodisperse spheres, then each sphere will be completely contained within its Voronoi cell. The volume fraction of the sphere inside its Voronoi cell has been proposed as a local measure of

density.^{43,44} For polydisperse spheres, a standard Voronoi tessellation is no longer a suitable tessellation since it is possible for the Voronoi cell to be completely embedded inside of a sphere. In the supplemental materials, we present two extensions of the Voronoi tessellation that are suitable for polydisperse spheres, the Voronoi S tessellation and the radical tessellation, and justify using the radical tessellation. We use a radical tessellation throughout the paper,⁴⁵ which is as computationally simple to calculate as the Voronoi tessellation. Like the Voronoi tessellation, the radical tessellation also decomposes space into irregular polyhedra with flat faces and straight edges. Each sphere of the polydisperse set will be completely contained within its radical cell.

Using the radical tessellation we introduce a novel way to study microphase-separated systems of multiple domains, which is discussed in more depth in the supplemental materials.[†] By summing the tessellation cells generated around one component type, we can calculate the volume of the domain containing that component. By dividing the volume of the measured domain by the volume of the components, we can calculate the packing fraction of a component within a domain. For example, for the TNS system we will sum the radical tessellation cells around the nanospheres to calculate the volume of the DG domain, and divide this volume by the net volume of the nanospheres to calculate a packing fraction.

We also use the radical tessellation to measure the local coordination or neighbor shell of each NS, which is discussed in more depth in the supplemental materials. We are interested only in the NS neighbors of a NS, and not the tether component, since the NS-NS interaction represents the important energetic interaction in the cooled system. Two NS are considered to be neighbors if the radical cells of the two nanospheres share a facet. We use this definition to calculate both how the system average NS coordination number (CN) is affected by polydispersity and how the NS CN depends on NS size as polydispersity is increased.

IV Results

A. Simulation results

Artificially grown double gyroids were generated by growing polydispersity into a DG structure that was previously formed under monodisperse conditions at $\phi = 0.30$ and 0.31 . We explored polydispersity values of $\Delta = 2, 4, 5, 6, 8, 10, 15, 20, 25$ and 30% . The double gyroid phase is found to be stable for $\Delta = 2, 4, 6, 8, 10\%$, and does not disassemble below $T^* = 0.31 \pm 0.1$, similar to the order-disorder temperature of the monodisperse DG phase.²² For $\Delta > 10\%$, we find that the double gyroid phase is stable (*i.e.* does not disassemble within 10^7 time steps) at low temperatures but disassembles at temperatures below the monodisperse order-disorder temperature. We find that double gyroids of $\Delta = 25\%$ disassemble above $T^* = 0.27 \pm 0.1$. Double gyroids of $\Delta = 30\%$ disassemble above $T^* = 0.26 \pm 0.1$.

Cooling tethered nanospheres generated self-assembled DG systems for ϕ from 0.285 to 0.315 . To remove any artificial bias from our system, we started from high temperature disordered configurations of polydisperse TNS. Nominal polydispersity values of $\Delta = 0, 2, 4, 5, 6, 8, 10, 12, 14, 15, 16, 18, 20, 24, 25$, and

30% were considered. SA polydisperse DGs formed at values of $\Delta = 0, 2, 4, 5, 6, 8, 10, 12, 14, 15, 18, 20, 24$ and 25% on cooling. For $\Delta > 20\%$, the DG phases generally disassembled within 10 million time steps unless cooled to below $T^* = 0.26$. Systems that did not form the DG were generally found to form hexagonally close packed cylinders (H), perforated lamellae (PL), an intermediate cylinder/perforated lamellae phase (H/PLH), or disordered wormy micelles (DWM). Both H and PL are the neighboring phases for the DG phase in the monodisperse TNS system²² and they are found at polydispersity levels where the gyroid did not form. The presence of H/PLH and DWM appears to be a TNS system kinetically trapped in a disordered state or oscillating between the H and PL phase. The order-disorder temperature of the SA polydisperse double gyroids for $\Delta < 10\%$ occurs at $T^* = 0.31 \pm 0.1$. The order-disorder temperature of the SA polydisperse DG for $\Delta > 10\%$ drops to $T^* = 0.26$ for $\Delta \geq 25\%$.

Fig. 3 shows the results of the phase diagram survey for $0.285 \leq \phi \leq 0.315$ and $0\% \leq \Delta \leq 30\%$, plotted in grid fashion with steps 0.005 in volume fraction and 5% in Δ . The relative proportion of the DG phase found at each concentration and (nominal) polydispersity is shown by darkness of shading. To be considered stable, we required that the phase in question persist for a minimum of 10 million time steps.

In this study, a single phase is almost never exclusively found at a state point due to kinetics and metastability. The distribution of alternate phases found (H, PL, and an intermediate H/PLH phase) can be found in the supplemental material. If the assembled structure in a simulation cell contained too many flaws (for example, screw dislocations, non-ordered connections between the cylinders or layers), the simulation was discarded as being not clearly identifiable. This is consistent with studying the self-assembly of small systems very close to the boundaries between phases. In the thermodynamic limit, we would expect only a single phase to be present. We observe that the H phase appears predominantly at lower volume fractions and the PL phase appears predominantly at higher volume fractions in the range examined. As polydispersity is increased, the cross-over volume

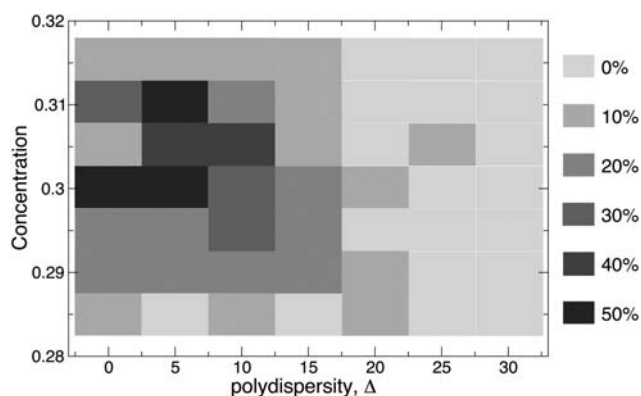


Fig. 3 A survey of the TNS phase diagram for $0.285 \leq \phi \leq 0.315$ and $0\% \leq \Delta \leq 30\%$, indicating the probability of observing the DG phase. The darkness of the shading indicates the fraction of the ten trials for which the DG phase was found. If multiple simulation box sizes were considered, the box size that produced most instances of the DG phase was used.

fraction from H phase to PL phase, as alternate phases, increases.

The DG phase appears to have a stability range of $\phi = 0.3 \pm 0.1$. We observe a peak in the presence of the DG phase for Δ between 5–10%. We also observe that for $\Delta > 15\%$, the DG phase self assembled more rarely, even when using a cooling schedule targeting self-assembly at $T^* = 0.25$. This may indicate that the ideal box size has shifted slightly, that DG with $\Delta > 15\%$ are kinetically difficult to form, or that the DG phase is no longer the free energy minimum phase for the system.

Fig. 4 shows properties of both the SA and AG systems as a function of polydispersity at $T^* = 0.256$ for $\phi = 0.3$; these properties are discussed in detail in the succeeding subsections. Fig. 4 also shows the same properties for the quasi-equilibrated AG system. Each data point in Fig. 4 represents a unique distribution of particle sizes drawn from the distribution function (2). Despite the different histories of how the double gyroid phase was generated, all the data is in good agreement. The correlations in potential energy and overall bulk structural trends between AG and SA DGs suggests that artificially adding polydispersity to a monodisperse system (*i.e.* growing the particles) can be used to rapidly assess the stability of a structure with relatively minimal computational cost. Also, the correlations between the order–disorder transitions found for SA DG and heated AG DG suggests that artificially adding polydispersity to a monodisperse system can also be used to estimate the polydisperse phase diagram with relatively minimal computational cost.

B. Polydispersity and the free energy minimum

In general, we expect the DG to self-assemble when the phase is a kinetically accessible, free energy minimum for the system. We consider NS polydispersity to have very little impact on entropic free energy terms; we find the radius of gyration of the tethers, for example, increases by less than half a percent when Δ is changed from 0 to 24%, smaller by a factor of two than the standard deviation. Thus, polydispersity primarily impacts the energetic interaction between the nanospheres.

In Fig. 4a, the contribution to the potential energy from the NS-NS interactions of the various polydisperse double gyroids is shown. This energetic interaction will be subsequently referred to as the potential energy (PE) of the system. We observe that the PE of the NS decreases as we increase polydispersity for $\Delta < 8\%$. For $\Delta > 8\%$, PE increases with increasing Δ . At $\Delta = 15\%$ the DG phase has a higher potential energy than the monodisperse state. We note that our parameter search found very few cases of DG for $\Delta > 15\%$. While the AG DG may be trapped in a metastable basin at higher polydispersity, the nanoparticles themselves are not frozen but are still actively exploring phase space. As can be seen from Fig. 5, at $T^* = 0.256$ the TNS are still diffusing through the gyroid domain. We observe that for all levels of polydispersity, individual NS occasionally detach from one network of the double gyroid and recombine with the other network. As the polydispersity of the system increases, there is a growing gap between the diffusion coefficient of the smallest particles and the largest particles. However, all the particles have a well-defined diffusion coefficient. For $\Delta > 10\%$ the diffusion

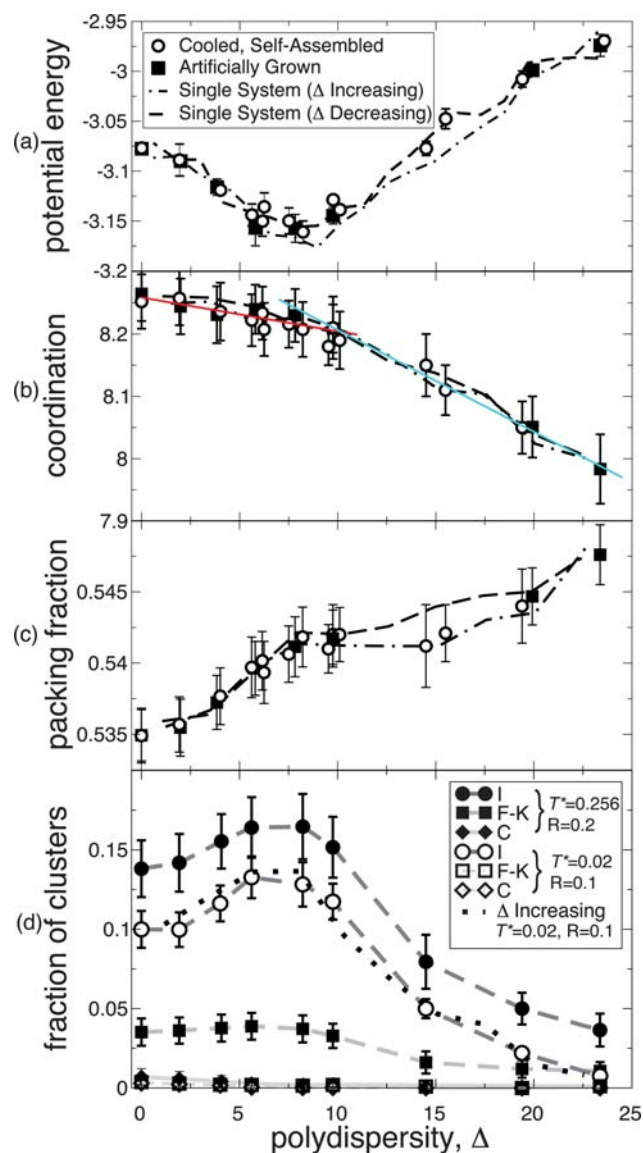


Fig. 4 Figure 4: Properties of the Double Gyroid (DG) phase are shown as a function of polydispersity (Δ) at $T^* = 0.256$ (unless otherwise indicated). Properties are shown up to 24% Δ , the maximum Δ for which the DG phase is stable at $T^* = 0.256$ when artificially grown. In (a) the potential energy (PE) based only on the NS-NS interaction is plotted. Artificially grown, quasi-equilibrated, and self assembled double gyroids all behave consistently with increasing Δ . In general the PE decreases until 8% Δ , and then increases. In (b), we calculate the average coordination number (CN) of the nanospheres. The CN decreases monotonically as Δ increases. The red and blue linear fits demonstrate the decrease becomes steeper after 8% Δ . In (c), we show the packing fraction of the NS in the domain of the gyroid (channels and nodes). Both (b) and (c) are generated from Voronoi tessellations (radical) of the DG domain. In (d) a RYLM local structural analysis is used to identify the proportion of icosahedral (I), Frank-Kasper (F-K), and crystalline (C) cluster motifs in the DG structure. The trends identified at $T^* = 0.256$ (closed shapes) and at $T^* = 0.02$ or quenched, (open shapes) are similar. The dotted line represents quenched quasi-equilibrated data for increasing polydispersity.

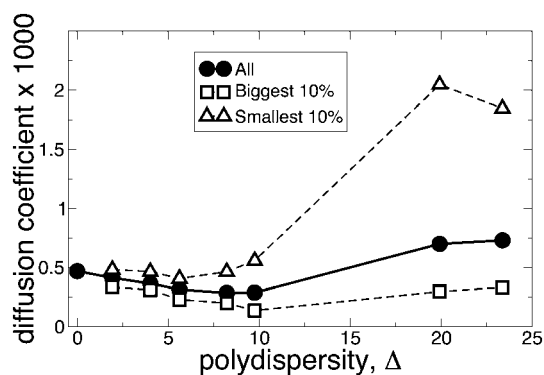


Fig. 5 The diffusion coefficients of the average, 10% smallest, and 10% largest NS are shown as a function of polydispersity. The y -axis is scaled by a factor of 1000. The dimensionless units are in $\sqrt{\epsilon/m}$.

coefficient of the larger particles increases, perhaps due to the lubricating presence of the fast moving smaller particles.

We note that the diffusion coefficient also shows a trend change at $\Delta \approx 8\%$. This trend change may be due to the increase in the potential energy of the structure; as particles become less likely to become caught in deep local energy minima, they diffuse through the system more freely. In Section IV.C we give a more detailed analysis of these deep local energy minima.

C. Local structure analysis of polydisperse gyroids

We can better understand the trends in polydispersity by analyzing the effect of polydispersity on the packing properties of the NS. We use the R_{YLM} analysis to identify the local structure, and calculate the average packing properties of the DG domain using a Voronoi (radical) tessellation.

i. Applying the R_{YLM} local structure analysis to the polydisperse gyroid phase. It was observed that in monodisperse TNS icosahedral structures are favored in systems of NS confined to cylindrical geometries where the relative diameter of the cylinder is less than 5, otherwise hcp/fcc crystalline arrangements form²². As previously noted, the DG phase is essentially composed of a series of interconnected cylindrical tubes. In the TNS system, the tether sterically restricts particle packing and the NS tend to pack into icosahedral and crystalline clusters with partial coordination (*i.e.* one coordination position of an ideal cluster must be unoccupied so that the central particle's tether can escape the local structure). The R_{YLM} method is used to match the pattern of bond angles between a particle and its nearest neighbors, or coordination shell, with a library of structural motifs. Iacovella *et al.*²² showed using the R_{YLM} method with a residual cutoff $R = 0.316$ that at $T^* = 0.256$, about 30% of the NS are central particles of a local structure that resembles an icosahedral cluster with partial coordination. Since Iacovella *et al.* also proposed that the local icosahedral packing stabilized the DG structure, it is of interest to consider how adding polydispersity to the system affects the local packing.

In this paper we utilize a lower cutoff of $R = 0.2$ at $T^* = 0.256$ and $R = 0.1$ at $T^* = 0.02$, creating a tighter tolerance than used in Ref. 22 for the structures we identify. In Fig. 4d, the local structure analysis of polydisperse gyroids is shown at $T^* = 0.256$

and quenched to $T^* = 0.02$, as well as the quasi-equilibrated AG system for increasing polydispersity at $T^* = 0.02$. We see that in all cases the trends are similar with a distinct peak in icosahedral ordering at $\Delta = 6\text{--}8\%$ and almost no icosahedral ordering at $\Delta = 20\%$. For $\Delta \geq 20\%$, the icosahedral packing motif is disrupted by polydispersity.

In general we note that polydispersity increases the dimensionality of the energy landscape for the NS. Individual NS are no longer interchangeable. However, for low levels of polydispersity most of the NS are still the same size and are approximately interchangeable, *i.e.* the energy difference caused by interchanging the particles should be small. We find the formation of icosahedral local packing is still dominant at low polydispersity. In fact, a low level of polydispersity promotes well-ordered icosahedral local structure, with the degree of icosahedrality peaking at approximately $\Delta = 6\text{--}8\%$. At higher polydispersity, the formation of local icosahedral packing is rapidly suppressed. We note that this trend is consistent with the idea that local icosahedral packing stabilizes the DG structure as local icosahedral packing becomes suppressed at roughly the same polydispersity level where the DG ceases to self-assemble readily from a disordered configuration (*i.e.* $\Delta > 15\%$).

In comparison, the presence of Frank-Kasper and crystalline local structure is largely unaffected by polydispersity. Since, neither local structure is a significant motif in the DG structure, as can be seen in Fig. 4d. The F-K clusters identified in Fig. 4d are most likely due to thermal noise in the bond-angle measurement.

ii. Analysis of low polydispersity promotion of local icosahedral packing. The key to understanding why low polydispersity would promote local icosahedral packing can be related to two observations: (1) The local structure of the monodisperse DG is characterized by icosahedral packing motifs, and (2) To the local structure, a low level of polydispersity implies most particles are the same size, with an occasional larger or smaller particle present. As such, we consider the impact of the presence of a single larger or smaller particle on the isolated icosahedral cluster.

Doye and Meyer studied the energy minimizing arrangements of isolated binary clusters, *i.e.* clusters of LJ particles of two different sizes.⁴⁶ They found that up to a diameter ratio of 1.1, the low-energy binary cluster formed by 9–13 LJ particles is a partial to full icosahedral cluster with all large particles in the shell and the small particle at the center. This arrangement is because the distance between atomic centers for neighboring atoms in the shell of an icosahedral monodisperse cluster is 5.15% larger than that for a central atom and a nearest neighbor atom. A 9.79% reduction in the diameter of the central atom relieves this strain,^{46,47} and an energy minimum of the binary icosahedral cluster occurs around this value. However, a further increase in the ratio of the diameters of the two species causes a change in the lowest-energy LJ cluster structure,⁴⁶ *i.e.* small particles begin appearing in the shell as well[‡], or the partial icosahedral

[‡] The full icosahedral cluster (coordination 12) has a shell of large particles around a small particle up to a binary diameter ratio of 1.15. At a ratio of 1.2, four of the shell particles become small, as the central particle is now too small for twelve large particles to fit around comfortably.

Table 1 A cluster analysis is performed on the energy minimizing binary clusters of Doye 2005,⁴⁶ and the Cambridge Cluster Database. For each binary cluster, an “I” is indicated if the cluster best matched a full or partial icosahedral cluster, or a “Z” for best matching a Frank-Kasper polyhedra. The χ value of the cluster match is also shown. For a coordination of 12, note that an icosahedral cluster and the Frank-Kasper polyhedra are identical

Coordination	Binary Ratio					
	1.05	1.10	1.15	1.20	1.25	1.30
8	I 0.091	I 0.103	I 0.097	I 0.130	I 0.146	I 0.149
9	I 0.056	I 0.017	I 0.070	I 0.147	Z 0.153	Z 0.146
10	I 0.040	I 0.014	I 0.196	I 0.208	I 0.261	Z 0.049
11	I 0.005	I 0.004	I 0.062	I 0.108	Z 0.147	Z 0.234
12*	I 0.001	I 0.105	I 0.115	I 0.217	I 0.198	I 0.219

structure becomes distorted. In Table 1, we perform a R_{YLM} analysis on the lowest-energy binary LJ clusters, and find the clusters progressively deviate from icosahedral bond angles and begin resembling other Frank-Kasper polyhedra as the binary ratio increases.

Following the work of Doye and Meyer, we would expect that for an icosahedral cluster with a single large particle, the large particle would tend to occupy the shell and not the center of the cluster; we would also expect the resulting cluster to be lower energy than an equivalent monodisperse cluster as the larger particle would help relieve strain.

We test this hypothesis by growing a set of NS with discrete binary polydispersity into a monodisperse DG structure. One “binary” DG was created with 10% of the NS having radii 10% larger and a second was created with 10% of the NS having radii 10% smaller. These binary DGs were created identically to the artificially grown DGs described in Section III at $T^* = 0.256$, and equilibrated at this temperature until the NS had, on average, diffused at least halfway across the simulation box. We find that small NS are 16 times more likely to be found at the center of local icosahedral structures than the large NS. The large NS were 1.3 times more likely to be found in a coordination shell than a small NS. Small NS and large NS promote local icosahedral structure by 2% and 15%, respectively. Small NS may also promote local icosahedral structures with slightly higher coordination; quenched local icosahedral structures had 4% higher coordination.

In general, we find that the presence of small NS lowers the potential energy of a given local icosahedral structure by creating a lower-energy, higher-coordination structure, while large NS, which relieve the strain in the coordination shell, encourage more local icosahedral structures to form. Thus, for a DG formed at low polydispersity levels, the minor fraction of smaller and larger NS are working in concert to lower the energy and further stabilize the DG structure. Fig. 4d shows that the fraction of well-ordered icosahedral clusters peaks at around a polydispersity of 6%. At this level of polydispersity, we find that a NS in the center of the local icosahedral structure is 5.6% smaller than its coordination shell NS.

D. Studying the average structure properties of the DG phase with the Voronoi tessellation

We use a generalized Voronoi tessellation, specifically the radical tessellation,⁴⁵ to determine how polydispersity affects the average

volume fraction of the gyroid domain and the average NS coordination number (see section IIIC and the supplemental material for more details[†]). As shown in Fig. 4c, we find that as the polydispersity of the system is increased, the gyroid domain becomes more densely packed, increasing from 0.535 at $\Delta = 0\%$ to 0.548 at $\Delta = 24\%$. This increase is a result of the extra degree of freedom in particle size, which permits the NS to locally arrange in tighter configurations. This is in good agreement with simulations of hard spheres, where variation in particle size is shown to increase the packing fraction.⁴⁸ Like the measure of potential energy, calculating the packing fraction of the DG is indifferent to how the polydisperse gyroid is formed. We note that while in monodisperse systems tighter sphere packing is associated with lower energy configurations, the ability of a polydisperse system to pack tighter than a monodisperse system does not necessarily imply that the polydisperse system must also have a lower energy than the monodisperse system. We find that packing fraction increases over the entire range of polydispersity (Fig. 4c) while potential energy initially decreases with increasing Δ up to $\Delta = 8\%$ and then increases with increasing Δ (Fig. 4a).

Fig. 4b shows that increasing polydispersity lowers the average NS coordination number of the system. Linear fits of the NS coordination as a function of the polydispersity below and above 8% are shown to illustrate the slope change that occurs with increasing polydispersity. The potential energy of the NS is a function of two properties, the coordination number of NS and the distance to each neighbor in the coordination shell. For $\Delta < 8\%$ we previously observed that PE decreases with increasing Δ (Fig. 4a); we additionally observe that the packing fraction of the DG increases rapidly but the average NS coordination number drops only slightly with increasing Δ . We conclude the system is lowering its PE by finding tighter configurations where more NS are sitting in the bottom of the potential energy wells of their neighbors, in a manner analogous to the isolated icosahedral cluster with a 9.7% smaller particle at its center. As the average NS coordination begins to drop more rapidly, the effect of this drop can be seen in the increase of potential energy shown in Fig. 4a. Although the average NS coordination decreases with increasing polydispersity, this decrease is not universal for all NS sizes, but represents a net effect. The fact that the net effect is negative may be due to sphere packing in a DG structure. In Fig. 6a, we show the coordination number for the NS in different polydisperse systems averaged over 20,000 time units and plotted against the diameter of each particle. As the polydispersity increases, the coordination number becomes a strong function of NS diameter. In Table 2, we show how average coordination trends with polydispersity and how the coordination becomes a stronger function of sphere size as polydispersity increases. The correlation coefficient, which measures the strength of the linear relationship between diameter and number of neighbors, increases significantly between $\Delta = 2, 10, \text{ and } 24\%$. As the potential energy of a shifted Lennard-Jones NS is a strong function of its coordination, in Fig. 6b we see that the average PE of each NS, averaged over the same elapsed time, decreases with NS diameter. It is also clear that for the more polydisperse DG, the vertical spread of potential energy values for a given diameter is a function of the particle diameter. This reflects the different diffusion coefficients for large and small particles in the same system, as shown in Fig. 5. That is, smaller NS, in shallower potential energy wells, diffuse faster through the system

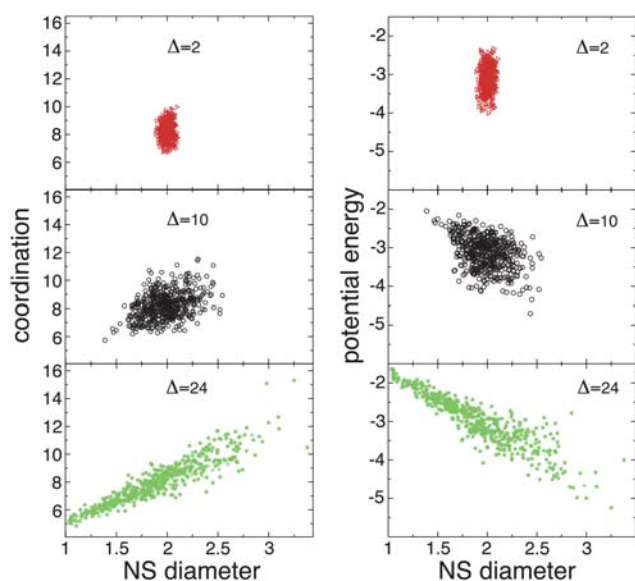


Fig. 6 Increasing polydispersity induces a spreading in the coordination number and potential energy of the NS as a function of NS diameter. In (a), the number of NS neighbors (averaged over 2×10^6 time steps) for each NS is shown. In (b), the potential energy (averaged over 2×10^6 time steps) for each NS is shown.

Table 2 An analysis is performed on the influence of polydispersity on the average coordination and the correlation between NS diameter and coordination for the data shown in Fig. 6

Polydispersity	Average NS coordination number	Correlation coefficient
2%	8.24 ± 2.00	0.080
10%	8.23 ± 2.02	0.395
24%	7.98 ± 2.25	0.922

and also explore the range of possible energy configurations faster, resulting in less spread in the measured potential energy for a small diameter.

We conclude that for low levels of polydispersity, the system is able to relieve internal packing frustration, *i.e.* NS are able to adjust so that more spheres are sitting in the bottom of the potential energy wells of other particles, lowering the energy of the system. For larger values of polydispersity, the net decrease in average NS coordination is responsible for the net increase in the potential energy of the system.

V. Conclusions

We have determined that tethered NS will readily form the gyroid phase for polydispersities up to 10% and has no terminal polydispersity as high as 30%. Polydisperse TNS with aggregating head-groups with polydispersities of $\sim 10\%$ form the DG phase at the same volume fraction ϕ (0.285–0.315) and temperature (0.31 ± 0.1) as the monodisperse TNS system. At this low level of polydispersity, the larger and smaller NS work together to create a larger number of lower energy icosahedral clusters which add to the stability of the DG. However, as polydispersity increases beyond 10%, the icosahedral structures in the DG become disrupted, the local structure becomes disordered, and

although the gyroid domain becomes more densely packed, the average nanosphere coordination number decreases. This results in a net increase in the potential energy of the system and thus for $\Delta > 10\%$, the DG phase self-assembles at a decreasing temperature and self-assembles more rarely. We conclude that above a polydispersity level of 10% the disruption of local icosahedral structure in the gyroid system has a strong impact on the free energy of the gyroid system and the phase becomes energetically more difficult to form.

If we compare the properties of polydisperse tethered LJ spheres confined to the NS domain to the properties of a bulk supercooled polydisperse LJ liquid, we find good agreement with some properties and disagreement with others. For both systems, initially increasing polydispersity lowers the diffusion coefficient,^{49,50} but for the TNS in the NS domain, at 10% polydispersity the diffusion coefficient begins to increase as a function of polydispersity. Also, while the coordination number of a polydisperse supercooled LJ liquid increases as a function of polydispersity,⁵⁰ for the TNS in a DG, the coordination number decreases. These differences are likely caused by a combination of the act of confining LJ spheres to a DG domain and the steric influence of the tether on the LJ sphere packing.

As to whether polydisperse gyroids will be able to be found in experiment, we observe that a polydispersity of 10% is within the range of values reported by some manufacturers of nanoparticles,^{28–30} but is a tighter tolerance than what other “monodisperse” nanoparticle synthesis methods can produce.^{51–53} Our simulations suggest that only NS manufactured at a polydispersities of up $\sim 10\%$ should be expected to form this phase, but that manufacturing to polydispersities less than 6% is unnecessary and may even lower the likelihood of finding this phase.

More generally, it is also apparent that polydispersity can have subtle but important impacts on the properties of sphere packing, especially in an unusual domain geometry. A relatively small amount of polydispersity can disrupt internal structures and change the per-particle energy of the packing. For sensitive phases, therefore, it can be critical to consider how much polydispersity a phase can tolerate before assuming the phase will be found in experimental systems.

Acknowledgements

We would like to thank Chris Rycroft for providing his Voronoi cell software that we then modified for use in this work and for providing helpful comments on the development of the polydisperse Voronoi methods. The 3D Voronoi Cell Software Library, Voro++, can be downloaded from <http://math.lbl.gov/voro++/>. We thank Joshua Anderson in the Glotzer group for his help with HOOMD-blue. HOOMD-blue can be downloaded from <http://codeblue.umich.edu/hoomd-blue/>. Research supported by the U.S. Department of Energy, Office of Basic Energy Sciences, Division of Materials Sciences and Engineering under Award DEFG02-02ER46000. CLP also acknowledges the DOE Computational Science Graduate Fellowship under DOE Grant DE-FG02-97ER25308. We thank the University of Michigan Center for Advanced Computing for support of our computer clusters. We are grateful to the NCSA and NERSC for computer time.

References

- C. Park, J. Yoon and E. L. Thomas, Enabling nanotechnology with self assembled block copolymer patterns, *Polymer*, 2003, **44**, 6725–6760.
- T. P. Lodge, Block copolymers: Past successes and future challenges, *Macromol. Chem. Phys.*, 2003, **204**, 265–273.
- M. J. Fasolka and A. M. Mayes, Block copolymer thin films: Physics and applications, *Annu. Rev. Mater. Res.*, 2001, **31**, 323–355.
- C. T. Black, K. W. Guarini, R. Ruiz, E. M. Sikorski, I. V. Babich, R. L. Sandstrom and Y. Zhang, Polymer Self assembly in semiconductor microelectronics, *IBM Journal of Research and Development*, 2007, **51**.
- M. P. Stoykovich and P. F. Nealey, Block copolymers and conventional lithography, *Mater. Today*, 2006, **9**, 20–29.
- J. Yoon, W. Lee and E. L. Thomas, Self-assembly of block copolymers for photonic-bandgap materials, *MRS Bulletin*, 2005, **30**, 721–726.
- Y. Fink, A. M. Urbas, M. G. Bawendi, J. D. Joannopoulos and E. L. Thomas, Block copolymers as photonic bandgap materials, *J. Lightwave Technol.*, 1999, **17**, 1963–1969.
- B. Jeong, Y. H. Bae, D. S. Lee and S. W. Kim, Biodegradable block copolymers as injectable drug-delivery systems, *Nature*, 1997, **388**, 860–862.
- G. S. Kwon, Block copolymer micelles as drug delivery systems, *Adv. Drug Delivery Rev.*, 2002, **54**, 167–167.
- Z. L. Zhang, M. A. Horsch, M. H. Lamm and S. C. Glotzer, Tethered nano building blocks: Toward a conceptual framework for nanoparticle self-assembly, *Nano Lett.*, 2003, **3**, 1341–1346.
- M. A. Horsch, Z. L. Zhang and S. C. Glotzer, Self-assembly of polymer-tethered nanorods, *Phys. Rev. Lett.*, 2005, **95**, 056105.
- S. C. Glotzer, M. A. Horsch, C. R. Iacovella, Z. Zhang, E. R. Chan and X. Zhang, Self-Assembly of anisotropic tethered nanoparticle shape amphiphiles, *Curr. Opinion Colloid Interface Sci.*, 2005.
- S. C. Glotzer and M. J. Solomon, Anisotropy of building blocks and their assembly into complex structures, *Nat. Mater.*, 2007, **6**, 557–562.
- A. Jayaraman and K. S. Schweizer, Effective Interactions, Structure, and Phase Behavior of Lightly Tethered Nanoparticles in Polymer Melts, *Macromolecules*, 2008, **41**, 9430–9438.
- S. Westenhoff and N. A. Kotov, Quantum Dot on a Rope, *J. Am. Chem. Soc.*, 2002, **124**, 2448–2449.
- K.-M. Sung, D. W. Mosley, B. R. Peelle, S. Zhang and J. M. Jacobson, Synthesis of Monofunctionalized Gold Nanoparticles by Fmoc Solid-Phase Reactions, *J. Am. Chem. Soc.*, 2004, **126**, 5064–5065.
- F. Huo, A. K. R. Lytton-Jea and C. A. Mirkin, Asymmetric Functionalization of Nanoparticles Based on Thermally Addressable DNA Interconnects, *Adv. Mater.*, 2006, **18**, 2304–2306.
- J. G. Worden, A. W. Shaffer and Q. Huo, Controlled functionalization of gold nanoparticles through a solid phase synthesis approach, *Chem. Commun.*, 2004, 518–519.
- G. A. DeVries, M. Brunnbauer, Y. Hu, A. M. Jackson, B. Long, B. T. Neltner, O. Uzan, B. H. Wunsch and F. Stellacci, Divalent metal nanoparticles, *Science*, 2007, **315**, 358–361.
- F. A. Aldaye and H. F. Sleiman, Dynamic DNA Templates for Discrete Gold Nanoparticle Assemblies: Control of Geometry, Modularity, Write/Erase and Structural Switching, *J. Am. Chem. Soc.*, 2007, **129**, 4130–4131.
- C. R. Iacovella, M. A. Horsch, Z. Zhang and S. C. Glotzer, Phase diagrams of self-assembled mono-tethered nanospheres from molecular simulation and comparison to surfactants, *Langmuir*, 2005, **21**, 9488–9494.
- C. R. Iacovella, A. S. Keys, M. A. Horsch and S. C. Glotzer, Icosahedral packing of polymer-tethered nanospheres and stabilization of the gyroid phase, *Phys. Rev. E: Stat., Nonlinear, Soft Matter Phys.*, 2007, **75**, 040801.
- C. R. Iacovella and S. C. Glotzer, Local ordering of polymer-tethered nanospheres and nanorods, *J. Chem. Phys.*, 2008, **129**, 044902.
- F. J. Martinez-Veracoechea and F. A. Escobedo, Lattice Monte Carlo simulations of the gyroid phase in monodisperse and bidisperse block copolymer systems, *Macromolecules*, 2005, **38**, 8522–8531.
- D. A. Hajduk, P. E. Harper, S. M. Gruner, C. C. Honeker, G. Kim, E. L. Thomas and L. J. Fetters, The Gyroid - A new equilibrium morphology in a weakly segregated diblock copolymers, *Macromolecules*, 1994, **27**, 4063–4075.
- M. A. Horsch, Z. L. Zhang, C. R. Iacovella and S. C. Glotzer, Hydrodynamics and microphase ordering in block copolymers: Are hydrodynamics required for ordered phases with periodicity in more than one dimension?, *J. Chem. Phys.*, 2004, **121**, 11455–11462.
- M. Maldovan, A. M. Urbas, N. Yulfa, W. C. Carter and E. L. Thomas, Photonic properties of bicontinuous cubic microphases, *Phys. Rev. B: Condens. Matter Mater. Phys.*, 2002, **65**, 165123.
- M. M. Maye, W. X. Zheng, F. L. Leibowitz, N. K. Ly and C. J. Zhong, Heating-induced evolution of thiolate-encapsulated gold nanoparticles: A strategy for size and shape manipulations, *Langmuir*, 2000, **16**, 490–497.
- M. Y. Ge, H. P. Wu, L. Niu, J. F. Liu, S. Y. Chen, P. Y. Shen, Y. W. Zeng, Y. W. Wang, G. Q. Zhang and J. Z. Jiang, Nanostructured ZnO: from monodisperse nanoparticles to nanorods, *J. Cryst. Growth*, 2007, **305**, 162–166.
- W. L. Pei, S. Kakibe, I. Ohta and M. Takahashi, Controlled monodisperse Fe nanoparticles synthesized by chemical method, *IEEE Trans. Magn.*, 2005, **41**, 3391–3393.
- P. G. Bolhuis and D. A. Kofke, Monte Carlo study of freezing of polydisperse hard spheres, *Phys. Rev. E: Stat. Phys., Plasmas, Fluids, Relat. Interdiscip. Top.*, 1996, **54**, 634–643.
- P. N. Pusey, The effect of polydispersity of the crystallization of hard spherical colloids, *J. Phys.*, 1987, **48**, 709–712.
- P. N. Pusey, in *Liquids, Freezing, and Glass Transition*, ed. D. Levesque, J.-P. Hansen and J. Zinn-Justin, 763–942.
- F. M. van der Kooij, K. Kassapidou and H. N. W. Lekkerkerker, Liquid crystal phase transition in suspensions of polydisperse plate-like particles, *Nature*, 2000, **406**, 868–871.
- R. P. Sear, Phase separation and crystallisation of polydisperse hard spheres, *Europhys. Lett.*, 1998, **44**, 531–535.
- M. A. Bates and D. Frenkel, Influence of polydispersity on the phase behavior of colloidal liquid crystals: A Monte Carlo simulation study, *J. Chem. Phys.*, 1998, **109**.
- G. S. Grest and K. Kremer, Molecular-Dynamics simulation for polymers in the presence of a heat bath, *Phys. Rev. A: At., Mol., Opt. Phys.*, 1986, **33**, 3628–3631.
- B. Widom, P. Bhimalapuram and K. Kenichiro, The hydrophobic effect, *Phys. Chem. Chem. Phys.*, 2003, **5**, 3085–3093.
- A. J. Schultz, C. K. Hall and J. Genzer, Obtaining Concentration Profiles from Computer Simulation Structure Factors, *Macromolecules*, 2007, **40**, 2629.
- M. Nonomura, K. Yamada and T. Ohta, Formation and stability of double gyroid in microphase-separated diblock copolymers, *J. Phys.: Condens. Matter*, 2003, **15**, L423–L430.
- P. J. Steinhardt, D. R. Nelson and M. Ronchetti, Bond-orientational order in liquids and glasses, *Phys. Rev. B: Condens. Matter*, 1983, **28**, 784–805.
- D. J. Wales and J. P. K. Doye, Global optimization by basin-hopping and the lowest energy structures of Lennard-Jones clusters containing up to 110 atoms, *J. Phys. Chem. A*, 1997, **101**, 5111–5116.
- C. H. Rycroft, *Multiscale Modeling in Granular Flow*, Thesis, Massachusetts Institute of Technology, 2007.
- C. H. Rycroft, G. S. Grest, J. W. Landry and M. Z. Bazant, Analysis of Granular Flow in a Pebble-Bed Nuclear Reactor, *Phys. Rev. E: Stat., Nonlinear, Soft Matter Phys.*, 2006, **74**, 021306.
- S. Sastry, D. S. Corti, P. G. Debenedetti and F. H. Stillinger, Statistical geometry of particle packings. 1. Algorithm for exact determination of connectivity, volume, and surface areas of void space in monodisperse and polydisperse sphere packings, *Phys. Rev. E: Stat. Phys., Plasmas, Fluids, Relat. Interdiscip. Top.*, 1997, **56**, 5524–5532.
- J. Doye, P. K. and L. Meyer, Mapping the magic numbers in binary Lennard-Jones clusters, *Phys. Rev. Lett.*, 2005, **95**, 063401.
- S. Cozzini and M. Ronchetti, Local icosahedral structures in binary-alloy clusters from molecular-dynamics simulation, *Phys. Rev. B: Condens. Matter*, 1996, **53**, 12040–12049.
- D. He, N. N. Ekere and L. Cai, Computer simulation of random packing of unequal particles, *Phys. Rev. E: Stat. Phys., Plasmas, Fluids, Relat. Interdiscip. Top.*, 1999, **60**, 7098.
- N. Kiriushcheva and P. H. Poole, Influence of mass polydispersity on dynamics of simple liquids and colloids, *Phys. Rev. E: Stat., Nonlinear, Soft Matter Phys.*, 2001, **65**, 011402.

-
- 50 S. E. Abraham, S. M. Bhattacharya and B. Bagchi, Energy landscape, antiplasticization, and polydispersity induced crossover of heterogeneity in supercooled polydisperse liquids, *Physical Review Letters*, 2008, **100**.
- 51 J. Salado, M. Insausti, d. M. I. Gil, L. Lezama and T. Rojo, Synthesis and magnetic properties of monodisperse Fe_3O_4 nanoparticles with controlled sizes, *J. Non-Cryst. Solids*, 2008, **354**, 5207–5209.
- 52 J. Vidal-Vidal, J. Rivas and M. A. Lupez-Quintela, Synthesis of monodisperse maghemite nanoparticles by the microemulsion method, *Colloids Surf., A*, 2006, **288**, 44–51.
- 53 W. Li, Facile synthesis of monodisperse Bi_2O_3 nanoparticles, *Mater. Chem. Phys.*, 2006, **99**, 174–180.
- 54 J. D. Weeks, D. Chandler and H. C. Anderson, Role of repulsive forces in determining equilibrium structures of simple liquids, *J. Chem. Phys.*, 1971, **54**, 5237–5247.